Heterosynaptic plasticity underlies aversive olfactory learning in Drosophila

Toshihide Hige[1,*], **Yoshinori Aso**[2], **Mehrab N. Modi**[1], **Gerald M. Rubin**[2], and **Glenn C. Turner**[1,*]

[1]Cold Spring Harbor Laboratory, Cold Spring Harbor, NY 11724, USA

[2]Janelia Research Campus, Howard Hughes Medical Institute, 19700 Helix Drive, Ashburn, VA 20147, USA

Summary

Although associative learning has been localized to specific brain areas in many animals, identifying the underlying synaptic processes *in vivo* has been difficult. Here, we provide the first demonstration of long-term synaptic plasticity at the output site of the Drosophila mushroom body. Pairing an odor with activation of specific dopamine neurons induces both learning and odor-specific synaptic depression. The plasticity induction strictly depends on the temporal order of the two stimuli, replicating the logical requirement for associative learning. Furthermore, we reveal that dopamine action is confined to and distinct across different anatomical compartments of the mushroom body lobes. Finally, we find that overlap between sparse representations of different odors defines both stimulus-specificity of the plasticity and generalizability of associative memories across odors. Thus, the plasticity we find here not only manifests important features of associative learning but also provides general insights into how a sparse sensory code is read out.

Introduction

Adaptability and plasticity are integral aspects of animal behavior. Elucidating the plasticity of sensory-motor processing that enables flexible behavioral choices based on previous experience is fundamental to our understanding of these systems. In Aplysia, elegant work has shown that plasticity of synaptic connections between sensory and motor neurons underlies associative learning behavior, providing one of the first examples of the cellular mechanisms connecting physiology and behavior (Hawkins and Byrne, 2015). In most nervous systems, however, sensory information is distributed across large populations of neurons and processed across multiple circuit layers before reaching motor output. As part of this process, stimulus-specific sensory information must be transformed into a format

---

*Correspondence: hige@cshl.edu (T.H.); turner@cshl.edu (G.C.T.).

useful for motor output, where more abstract information such as the valence of stimuli are more relevant (Aso et al., 2014b; Hige et al., 2015; Owald et al., 2015). How then do neural circuits flexibly assign valence to different stimuli through learning? In the amygdala, fear or reward conditioning triggers synaptic plasticity in distinct populations of neurons that are implicated in negative- or positive-valence coding (Janak and Tye, 2015). However, since the amygdala receives converging input from multiple cortical areas as well as higher-order association areas, it has been challenging to follow the progressive steps of sensory transformations, and determine the impact of plasticity on that processing.

In contrast, the Drosophila brain offers the hope of a golden mean between these two extremes, as it uses population-level sensory coding, yet retains a simpler, more well-defined circuit organization in comparison to vertebrates. Pavlovian olfactory conditioning in Drosophila has also been a long-standing model for understanding the neural basis of associative learning. Behavioral genetics has identified a brain area known as the mushroom body (MB) as an important learning center (Heisenberg, 2003; Keene and Waddell, 2007; McGuire et al., 2005). The strengths of this system are that the neuronal architecture has been comprehensively mapped (Aso et al., 2014a; Mao and Davis, 2009; Tanaka et al., 2008), and that the sensory representations of the MB intrinsic neurons, the Kenyon cells (KCs), are well-characterized (Honegger et al., 2011; Turner et al., 2008). Then what is known about the learning-related plasticity in this circuit? In other insects, it has been shown that electrical stimulation paradigms can induce plasticity at MB output in locusts (Cassenaer and Laurent, 2007; 2012), and bees (Oleskevich et al., 1997), where learning-related changes have also been seen (Mauelshagen, 1993; Okada et al., 2007). In Drosophila, calcium imaging has revealed learning-related changes on either side of this synapse. While odor-evoked calcium signals increase in KC axons (Akalal et al., 2010; 2011; Boto et al., 2014; Tomchik and Davis, 2009; Wang et al., 2008; Yu et al., 2006, but see Zhang and Roman, 2013), signals in MBONs decrease in some cases (Owald et al., 2015; Séjourné et al., 2011) and increase in others (Bouzaiane et al., 2015; Owald et al., 2015; Pai et al., 2013; Plaçais et al., 2013). Regardless of the lack of consistency in the direction of these changes, all these results nonetheless point to the fact that the output site of the MB is a strong candidate for plasticity during learning. Furthermore, odor-tuning patterns of some MBONs are diverse across naïve animals, suggesting that MBON responses are individualized through experience-dependent plasticity (Hige et al., 2015). Despite these advances, this model system still surprisingly lacks an understanding of learning at the synaptic level. In this study, we describe a form of synaptic plasticity at the site of MB output that underlies aversive olfactory learning *in vivo*.

Aversive olfactory conditioning involves pairing an olfactory stimulus (conditioned stimulus, CS) with a noxious unconditioned stimulus (US). These two signals converge in the MB, where the CS is represented by KCs and transmitted to MBONs, while US signaling is mediated by dopaminergic neurons (DANs) that innervate the MB (Aso et al., 2012; 2010; Claridge-Chang et al., 2009; Mao and Davis, 2009; Pech et al., 2013; Riemensperger et al., 2005; Schroll et al., 2006; Schwaerzel et al., 2003). The neurites of these three neuronal elements present an intriguing arrangement in the MB lobes, the output site of the MB formed of parallel bundles of KC axons. The dendrites of each MBON type

occupy a specific subregion of the MB lobes (Aso et al., 2014a; Ito et al., 1998; Tanaka et al., 2008). Different MBON types tile the length of the KC axons, forming a total of 15 non-overlapping compartments (Figure 1A). In each of these compartments, MBON dendrites overlap with axonal projections of different DANs, which tile the lobes in a corresponding manner. Thus, each DAN is ideally located to heterosynaptically modulate KC output synapses onto a specific MBON partner, a notion that has been the basis for an important model for learning in Drosophila (Heisenberg, 2003). In fact, dopamine receptors in KCs play a crucial role in associative learning (Kim et al., 2007; Qin et al., 2012). Our goal in this work is to test this influential model by directly examining synaptic changes at this layer of the circuit.

Another prominent hypothesis inspired by this anatomy is that each MBON-DAN compartment represents a functionally independent unit. One of the striking results is that it is possible to train an animal by substituting US delivery with direct activation of DANs (Aso et al., 2010; Burke et al., 2012; Claridge-Chang et al., 2009; Liu et al., 2012; Schwaerzel et al., 2003), and the axonal projections of DANs responsible for appetitive and aversive memory are segregated in the MB lobes (Perisse et al., 2013). Furthermore, the MB, like the amygdala, is intimately involved in valence coding, as activating particular MBONs evokes attraction or avoidance, depending on which compartment they innervate (Aso et al., 2014b; Owald et al., 2015). This suggests a model where learning leads to a change in neural activity in the direction predicted from the valence of the MBON and the quality of the association. Indeed a recent study showed that, in a particular compartment that signals negative valence, the response to a conditioned odor is reduced relative to a control odor after reward learning (Owald et al., 2015). These findings raise important questions about the underlying synaptic and circuit mechanisms. In particular, it is of great interest to examine the role dopaminergic neurons play in the induction of plasticity and how this influences valence signaling by the MBONs. More fundamentally, it is not known whether synaptic strength can be independently modulated across different compartments, or whether the remarkable anatomical arrangement of the circuit really reflects its physiology. In order to address these questions, it is essential to manipulate DANs in a compartment-specific manner. In this study, we utilized new genetic tools to differentially label specific types of DANs. Combined with optogenetics, this enabled us to exert precise spatiotemporal control over the activity of DANs in the MB.

Finally, we addressed a general question about the stimulus-specificity of learning, exploiting existing knowledge about the representation of sensory information in the MB. As the third order neurons of the olfactory circuit, KCs have been an excellent model for studying sparse sensory representations. Each KC is narrowly tuned to odors, and a given odor elicits responses from a sparse ensemble of KCs (Honegger et al., 2011; Murthy et al., 2008; Perez-Orive et al., 2002; Turner et al., 2008), resembling the representations in pyramidal neurons in piriform cortex, again the third order neurons in vertebrate olfactory circuits (Stettler and Axel, 2009). The sparse format has been theoretically predicted to be useful for accurate memory formation since it minimizes the overlap between the sets of cells responding to different stimuli, making it easier to update synaptic strength in one stimulus pathway without interfering with the synapses used to represent other stimuli (Olshausen and Field, 2004). Indeed previous work has shown that overlap is related to

accuracy of memory formation (Campbell et al., 2013; Lin et al., 2014a). By studying plasticity at the output of KCs, we directly test this hypothesis. Thus, our study not only reports the first demonstration of synaptic plasticity in this important model circuit for learning and memory, but also addresses the more general question of how a sparse sensory code is read out.

Results

Long-lasting Suppression of MBON Responses Induced by Odor-Dopamine Pairing

We first focused on the γ1pedc compartment since it is critically involved in acquisition of aversive memory and therefore is most likely to exhibit plasticity. Thermogenetic activation of DANs innervating γ1pedc (PPL1-γ1pedc, or MB-MP1) effectively substitutes for US delivery, such that pairing activation with odor presentation is sufficient for flies to form an aversive association with that smell (Aso et al., 2010; 2012). Furthermore, blocking synaptic output of either PPL1-γ1pedc or MBON-γ1pedc (MB-MVP2), an output neuron of γ1pedc, disrupts aversive olfactory memory (Aso et al., 2010; 2014b). To examine the effect of odor-dopamine pairing on MBON responses, we made *in vivo* whole-cell recordings from MBON-γ1pedc, while pairing odor with optogenetic activation of PPL1-γ1pedc. To maximally restrict expression of the optogenetic exciter CsChrimson (Klapoetke et al., 2014), we created the split-GAL4 line MB320C, which labels a single PPL1-γ1pedc neuron (Figure S1A). Using this selective driver, we successfully trained flies using optogenetic DAN activation as a substitute for an aversive US in a behavioral assay with an olfactory arena (Figures S1C-S1H). For electrophysiological experiments, we added a LexA driver to label MBON-γ1pedc in the same brain (Figure 1B).

Prior to pairing, MBON-γ1pedc responded to our two test odors, 3-octanol (OCT) and 4-methylcyclohexanol (MCH), with high spike rates that persisted throughout the duration of the 1-s odor pulse (Figure 1D). We then carried out a single pairing of OCT (CS+; duration, 1 s) with four pulses of 1-ms light (2 Hz; Figure 1C), which evoked reliable spike trains in PPL1-γ1pedc (Figure S2). After this brief pairing, we observed a profound suppression in the MBON response to the CS+ (pre-pairing: 118 ± 8.3 spikes, post: 24 ± 7.4, mean $\pm$ SEM; $n = 7$), while the unpaired odor (MCH; CS-) was minimally affected (Figures 1D-1F; pre: 110 ± 11 spikes, post: 83 ± 14). We observed an equivalent effect when we used MCH as CS+ and OCT as CS− (Figure S3). The suppression persisted throughout the duration of the recordings, which lasted at least 40 min, and showed only a small sign of recovery in that time (Figure S4). In flies lacking the driver but otherwise genetically identical, odor-light pairing did not change odor responses (Figure S5), indicating that this suppression indeed depends on DAN activation mediated by CsChrimson. Thus, a very brief pairing of odor presentation with DAN activation induces a robust, stimulus-specific long-lasting suppression. Note that when we tested a much longer pairing protocol that is typically used in behavioral assays in flies (1min odor with 120 light pulses), we observed a similar, stimulus-specific suppression (Figures S6A-S6E).

CS-US Temporal Specificity

Associative learning requires a precise temporal relationship between CS and US; odor onset must precede the delivery of punishment. To examine whether the induction rule for plasticity in MBON-γ1pedc accounts for this core feature of associative learning, we tested a backward pairing protocol, where we delivered punishment (i.e. DAN activation) prior to odor onset (Figure 1G). We used the same number of light pulses as before, but instead started odor delivery 0.5 s after the last pulse of light. We observed no change in odor responses with this protocol (Figures 1H and 1J). Thus the strict timing requirement dictated by the logic of associative learning is implemented in the temporal properties of the underlying plasticity itself.

Odor-Dopamine Pairing does Not Change KC Odor Responses

The site responsible for the dramatic reduction in MBON-γ1pedc odor responses could be at the KC-MBON synapses, or somewhere upstream. Since our manipulation specifically activates DANs that innervate the axon terminal regions of KCs, we considered it unlikely that the pairing affects the input to the KCs. However, it is still possible that pairing has cell-wide effects on KCs, such as changes in their intrinsic excitability, that could greatly reduce their odor responses. To test this possibility, we used two-photon calcium imaging to compare KC responses before and after pairing. Since MBON-γ1pedc is potentially connected to α/β and γ KCs, which collectively amount to over 80 % of the whole KC population (Aso et al., 2014a; 2009), we used a pan-KC LexA driver (R13F02-LexA) to express GCaMP6f. As reported previously (Campbell et al., 2013), OCT and MCH evoked calcium responses in sparse, partially overlapping ensembles of KCs (Figures 2A and 2B). After pairing odor presentation with PPL1-γ1pedc activation using our 1-s protocol, response magnitudes of individual cells decreased slightly for both CS+ and CS− (Figures 2C-2F). However the magnitude of the decrease was indistinguishable between the two odors. Moreover, we observed a similar decrease when we omitted photostimulation (Figures 2E-2F), indicating that these small reductions are unrelated to the pairing. To see if there is any change in the representation patterns apart from the response magnitude, we analyzed how the population activity pattern changed before and after pairing (Figures 2G and 2H, see also Experimental Procedures). Again, we did not observe any CS+-specific change in response patterns. Furthermore, to directly test if KC excitability is changed by pairing, we recorded specifically from γ KCs using whole-cell patch clamp. Since it was difficult to target odor-responding KCs because of their sparsely responding nature, we mimicked odor responses by inducing spikes with current injection (Figure S7). Pairing KC depolarization with PPL1-γ1pedc activation did not change the spike threshold or the sustained spike rate (Figure S7). From these results, we conclude that the long-lasting suppression we observed in MBON-γ1pedc cannot be explained by either changes in odor responses in KCs or in their intrinsic excitability.

Odor-Dopamine Pairing Induces Synaptic Depression of MBON input

We next asked if synaptic input to MBON-γ1pedc is changed during long-lasting suppression. To test this, we measured excitatory postsynaptic currents (EPSCs) using voltage-clamp recordings (Figure 3A). We observed large odor-evoked EPSCs that typically

exceeded 200 pA in amplitude and were sustained throughout the duration of the odor pulse. After 1-s pairing of odor presentation and PPL1-γ1pedc activation, the EPSCs showed a marked depression in a stimulus-specific manner, with the current dramatically reduced early in the response, and essentially no sustained current visible at later time points (Figures 3B-3D). The average reduction in charge transfer was 90 ± 3.7 % (mean $\pm$ SEM; Fig 3D), which is of similar order to the 80 ± 5.7 % reduction in spiking we observed (Figure 1F). Combined with the evidence showing KC excitability is not altered by pairing, these results indicate that KC-MBON synapses undergo long-term depression (LTD) when co-activated with dopamine input. However, we do not rule out the possibility that there are other circuit elements presynaptic to the MBONs that may also contribute to the plasticity we observe here.

Plasticity is Independent of Postsynaptic Spiking

In locust, KC-MBON synapses undergo Hebbian spike-timing-dependent plasticity (STDP) (Cassenaer and Laurent, 2007). The neuromodulator octopamine, which is thought to mediate reward signaling (Burke et al., 2012; Hammer, 1993), modifies those synapses by changing the STDP rule (Cassenaer and Laurent, 2012). In this system, postsynaptic spikes play a critical role in the induction of plasticity. However, in behavioral experiments in Drosophila, flies still learn effectively when synaptic output of α/β and γ KCs is blocked during CS-US pairing (Dubnau et al., 2001; Krashes et al., 2007; McGuire et al., 2001), which suggests the existence of a plasticity-induction mechanism that does not require MBON spikes. The voltage-clamp experiments shown in Figure 3 strongly support this idea, since we observed clear LTD even though MBON spikes were completely suppressed by including the sodium channel blocker QX-314 in the patch pipette solution. However, this result leaves open the possibility that MBON spikes may partially contribute to the depression we observed in the spike rates. To test this possibility, we next recorded both spikes and EPSCs in the same cells by switching between current-clamp and voltage-clamp modes without QX-314. Odor-light pairing was performed in voltage-clamp mode (Figures 4A and 4B). This suppressed odor-evoked spikes by 83 ± 4.5 % (mean $\pm$ SEM, $n = 6$). In this condition, we still observed a similar level of depression in spike rates (Figures 4C-4E) as we observed after pairing in current-clamp mode (Figures 1D-1F). Importantly, EPSCs also underwent a similar degree of LTD (Figures 4F-4H) to that we observed with complete block of spiking (Figure 3). Together, these results indicate that MBON spikes do not contribute to this form of plasticity, consistent with previous behavioral studies.

Spatially Compartmentalized Plasticity in the MB Lobes

The remarkably compartmentalized organization of the MB lobes raises the possibility that each of the MBON-DAN modules is a functionally independent unit. This predicts that activity of an MBON in one compartment should not be altered by activating DANs that innervate a neighboring compartment. We tested this by examining whether MBON-γ1pedc activity is modified by pairing odor with activation of PPL1-γ2α'1, a DAN that projects to the adjacent γ2 compartment (as well as α'1). To optogenetically control this DAN, we created the split-GAL4 line MB099C, which labels four types of PPL1 DANs: PPL1-γ2α'1, α'2α2, α'3 and α3, but never labels PPL1-γ1pedc (Figure S1B). When we performed odor-light pairing using MB099C to drive CsChrimson (Figures S2B-S2D), odor responses of

MBON-γ1pedc were unaltered (Figures 5A-5D). On the other hand, when we activated a broader population of DANs including PPL1-γ1pedc using TH-GAL4, the pairing induced robust depression (Figures 5E-H). These results demonstrate that the dopamine released in one compartment of the MB lobe does not spill over into the next compartment to induce plasticity.

However, each KC axon makes en passant synapses with multiple MBONs in different compartments. Does the functional independence still hold for MBONs that share the same input KCs when plasticity is induced in one of the compartments? To test this, we recorded from MBON-γ2α'1 while inducing LTD in the adjacent γ1pedc compartment (Figure 5I). We did not observe any change in the odor responses in MBON-γ2α'1 (Figures 5J-5L), even though we know that robust LTD is induced in MBON-γ1pedc in the same conditions (Figures 1D-1F). Thus, the anatomically defined compartments of the MB lobes are indeed functionally independent.

Plasticity Rules Differ across Compartments

Do the DAN-MBON pairs in the MB lobes represent a series of functionally identical units each operating with the same plasticity rule? If so, then the pairing protocol that induced LTD in the γ1pedc compartment should be effective in the other modules as well. We tested this in the α2 compartment, where we recorded from MBON-α2sc and looked at the effects of activating the corresponding DAN by expressing CsChrimson in PPL1-α'2α2 using MB099C (Figure 6A). In this case, the 1-s odor-light pairing protocol that induced robust LTD in the γ1pedc compartment failed to induce any change in the MBON-α2sc odor response (Figures 6B-6D). We confirmed that light pulses effectively evoked spikes in PPL1-α'2α2 in these flies (Figure S2B). Thus, the action of dopamine is not identical across different compartments. Since previous work has shown that the average activity of the MB-V2 cluster of MBONs, which includes MBON-α2sc, shows a decrease in the relative response to CS+ and CS− odors after training with electric shock (Séjourné et al., 2011), it is certainly possible that PPL1-α'2α2 could induce plasticity under a different stimulation regime. Furthermore, our behavioral assay showed that optogenetic DAN activation using MB099C can serve as an aversive US, even though the efficacy is much lower than using MB320C to specifically activate PPL1-γ1pedc (Figure S1F). We therefore tested whether a longer pairing protocol can induce plasticity in the α2 compartment. We used pairing protocol with 1-min odor delivery and 120 photostimulation pulses (Figure 6E). With this protocol, we observed a robust, stimulus-specific LTD (Figures 6F-6H), similar in magnitude to that we saw in MBON-γ1pedc. Thus, dopamine released in α2 and γ1pedc compartments can induce similar plasticity, but clearly there are different rules governing plasticity in those two compartments.

Synaptic Interference and Olfactory Generalization

KCs have very odor-specific responses and different odors evoke responses from sparse, largely non-overlapping sets of KCs (Honegger et al., 2011; Perez-Orive et al., 2002; Turner et al., 2008). However, these sparse representations are immediately transformed into a dense format in the next layer where KCs converge onto a small number of MBONs (Cassenaer and Laurent, 2012; MacLeod et al., 1998). What then is the possible benefit of

having a sparse coding layer right before the heavy convergence? One theoretical prediction is that the sparse format is useful for accurate memory formation because updating synaptic strength in one stimulus pathway would not interfere with the synapses used to represent the other stimuli (Olshausen and Field, 2004), a problem known as synaptic interference. Indeed it was the case that the plasticity we observed was stimulus specific. However, it was not perfectly so - reciprocally pairing either OCT or MCH with DAN activation also slightly but significantly depressed responses to the other odor (Figures 1E and 1F and Figure S3). This may reflect a small degree of overlap in the representations of these two odors (33 % of MCH-responding KCs and 30 % of OCT-responding KCs respond to both these odors); there may simply be a practical limit to how effectively sparse coding can relieve synaptic interference even with such different odors. If so, this predicts that the greater the overlap between the sets of KCs responding to different odors, the greater the interference.

To test this possibility, we used a series of four odors with known levels of overlap in the KCs, to determine whether there was a corresponding degree of synaptic interference in our US-substitution experiments (Figures 7A and 7B). The four odors were pentyl acetate (PA), butyl acetate (BA), 2-heptanone (HP) and ethyl lactate (EL). Three of these, PA, BA and HP evoke similar, highly overlapping patterns of responding KCs, while EL elicits a very distinct response pattern (Campbell et al., 2013). We first tested for synaptic interference by pairing PA with photostimulation of PPL1-γ1pedc. In this set of experiments, we used 1-s odor pulses with just a single pulse of 1-ms light for pairing (Figure S6F). This milder protocol induced robust LTD to CS+ responses, while the effects on CS− responses were slightly less than the four-pulse protocol we used previously (20 ± 6.3 %, mean $\pm$ SEM; Figures S6G-S6I versus 27 ± 7.1 %; Figure 1). Pairing with PA effectively induced LTD not only for this odor, but also for the odors with overlapping KC representations, BA and HP (Figures 7C-7E). Despite this milder pairing protocol, the magnitude of depression for BA and HP was only marginally less than PA. On the other hand, EL responses were unaffected. Conversely, when we paired EL with PPL1-γ1pedc stimulation, the EL response underwent strong depression, while responses to the other three odors changed very little (Figures 7F-7H). We found that the extent of overlap between the KC response patterns for CS+ and these different tested odors was highly correlated with the magnitude of the depression (Figure 7I). In previous behavioral experiments using electric shock reinforcement, we established that flies generalize among these three odors - an association with one stimulus affects behavioral responses to the others (Campbell et al., 2013). We confirmed this here using our US-substitution approach (Figures 7J and 7K). Thus our results demonstrate that the generalization of odors, predicted from the similarity of the underlying KC response patterns, was indeed mediated by synaptic interference.

Discussion

In this study, by developing new tools for precisely manipulating neural circuitry in Drosophila, we provide the first characterization of synaptic plasticity linked to associative learning at the output of the MB. Focusing on the γ1pedc compartment, which is critically involved in memory acquisition, we observed long-term depression of the synaptic inputs to these MBONs. The fact that we see a roughly 90% reduction in synaptic currents supports the interpretation that the effect is at KC-MBON synapses, which are expected to be the

most prominent input to the MBONs. However, there is still the possibility that other circuit elements presynaptic to the MBONs, including potentially the DPM neuron that widely innervates the MB lobes (Keene et al., 2004), also contribute to the changes we see here. The plasticity was robust, long-lasting and depended on the temporal order of CS and US with sub-second precision. Thus, the minimum logical requirements for associative learning are implemented by dopamine-induced heterosynaptic plasticity.

Plasticity and Valence Coding by MBONs

MBONs have been proposed to convey the valence of olfactory stimuli, since direct activation of different MBONs can elicit approach or avoidance behavior, depending on the cell type (Aso et al., 2014b; Owald et al., 2015). In particular, MBON-γ1pedc is thought to signal positive valence, since optogenetically activating this neuron evokes attraction to the light (Aso et al., 2014b). If the plasticity is related to the behavior, then when an animal learns to avoid an odor, the response of MBON-γ1pedc to that particular odor should go down. Indeed, the plasticity we found in this neuron during aversive learning was LTD, and it was odor specific. Thus, these observations provide a simple, unifying explanation for how behavior is modified during learning.

In general, the direction of the behavioral response triggered by MBON activation (i.e. approach versus avoidance) is opposite in sign to the valence signaled by the corresponding DANs (i.e. reward versus punishment) (Aso et al., 2014b). This opponent relationship suggests that dopamine-induced plasticity is depression, so that DANs act by turning down activity of MBONs that signal the opposite valence (Owald et al., 2015). We indeed found that heterosynaptic LTD takes place not only in the γ1pedc compartment but also in α2. However, our results also indicate that the rules for inducing plasticity are not the same across all compartments, as it required much longer pairing of odor and DAN activation to induce plasticity in the α2 compartment than in γ1pedc. What is the functional significance of this differential sensitivity to dopamine? The extremely high sensitivity in the γ1pedc compartment matches well with the observations that activation of PPL1-γ1pedc can substitute aversive US at much higher efficiency compared to other PPL1-DANs (Figure S1F; (Aso et al., 2010; 2012). Although the difference in these behavioral scores could potentially be explained by other factors such as differential strength of the link from the MBON to behavioral output, it is consistent with the fact that the γ1pedc compartment (Aso et al., 2010; 2014b) or, more generally, γ KCs (Blum et al., 2009; Qin et al., 2012) play a critical role in acquisition of aversive memory. On the other hand, the behavioral evidence suggests the α2 compartment may be more heavily involved in retrieval of memories (Bouzaiane et al., 2015; Séjourné et al., 2011).

Compartmental Specificity of Dopamine Signaling

Our results show that the anatomically defined MBON-DAN modules in the MB lobes reflect the modularity of circuit function, compartmentalizing the synaptic changes that accompany learning into these discrete zones. This matches well with the picture developed from recent behavioral studies indicating the different compartments are related to distinct motivational drives (Burke et al., 2012; Huetteroth et al., 2015; Krashes et al., 2009; Lin et al., 2014b; Liu et al., 2012; Musso et al., 2015; Yamagata et al., 2014). These studies

showed that the dopaminergic neurons required for learning with different types of reinforcement project to different compartments. For example, the DANs necessary and sufficient for appetitive conditioning project to different compartments than learning driven by thirst (Lin et al., 2014b). Even reinforcement by sweet taste versus caloric intake are localized to distinct compartments (Huetteroth et al., 2015). These studies lead to the hypothesis that there is a mechanism whereby information represented by the MB is independently read out by multiple types of MBONs. Our results here provide the first evidence that this is achieved by compartmentalizing the synaptic changes driven by different reinforcement pathways into these discrete anatomical zones. Dopamine released in one compartment induces robust plasticity in that compartment but not in its neighbor. This modularity is all the more noteworthy, since the dopamine receptors involved in memory acquisition reside in the KC axons (Kim et al., 2007; Qin et al., 2012), and each KC axon makes en passant synapses with dendrites of multiple MBONs in different compartments. Nevertheless, we find that the action of dopamine is spatially well-confined – even though MBON-γ1pedc and MBON-γ2α'1 likely share most of the same KC inputs, inducing plasticity in the γ1pedc compartment does not alter the responses in γ2α'1. This indicates that neither dopamine nor its downstream intracellular signaling molecules can spread into the synaptic boutons of the same KC axon in the very next compartment. The circuit organization of the MB represents an ideal format for the parallel read out of information, since large numbers of KCs make converging connections with multiple MBONs at different points down the length of their axons. Thus, each MBON likely has access to much of the olfactory information present in the KC population. The compartmentalization of plasticity would allow the circuit to form a series of different, highly-odor specific associations in each of the MBON-DAN modules, making it possible for the flies to make the complex context-dependent choices they need to cope with a changing environment.

The compartmental specificity we see here is broadly consistent with previous observations that thermogenetically activating DANs leads to an elevation in cAMP levels in KC axons that is localized to the specific compartments innervated by those DANs (Boto et al., 2014). Moreover, abundant genetic evidence suggests that cAMP signaling is central to induction of plasticity in the MB (Davis, 2005). However, Boto et al. (2014) did not observe any change in odor-evoked calcium responses in the KC axons in the γ1 region after pairing odor with DAN activation using TH-GAL4, even though we observed very robust LTD in MBON-γ1pedc using the same GAL4 line (Figures 5E-5H). In fact, there was not a close correlation between the spatial patterns of cAMP elevation and of altered calcium responses; some compartments that did not show a cAMP elevation exhibited a change in odor-evoked calcium responses, while other compartments that did show cAMP increases did not show a change in calcium responses (Boto et al., 2014). This lack of correlation might arise simply because the molecular machinery used for plasticity lies downstream of calcium influx, or it may be that the change in calcium concentration is so small and local that it is difficult to detect with a cytosolic calcium reporter. It is also possible that plasticity is predominantly expressed postsynaptically. Several pioneering studies have demonstrated learning-related changes in odor responses of KC axons using calcium imaging (Akalal et al., 2011; Wang et al., 2008; Yu et al., 2006; Zhang and Roman, 2013). Given the possible discrepancy

between synaptic plasticity and changes in axonal calcium signals, this issue needs further investigation.

Reading Out a Sparse Sensory Code

Much like other higher-order sensory areas, stimulus representations in KCs involve sparse activation of small numbers of cells, each of which has highly specific response properties. Having established methods to induce plasticity in a neuron that receives heavily converging input from a well-characterized sparse coding area, we had a unique opportunity to directly test a long-held hypothesis about sparse coding. That is, by reducing the overlap between ensembles of cells responding to different stimuli, sparse representations minimize the problem of synaptic interference. By testing multiple odor pairs that evoke similar or dissimilar responses in the KC population, we indeed found a clear relationship between the degree of overlap in KC representations and the odor specificity of the plasticity. These results suggest a simple model for learning, where those KC-MBON synapses that are active upon the arrival of dopamine (or shortly prior to its arrival) undergo plasticity. Our observation that plasticity does not rely on MBON spiking also supports the idea that it is the coincident activity of KCs and DANs that is the sole determinant for plasticity. When these synapses overlap with those activated by similar odors, the stimulus-specificity is concordantly reduced.

Our parallel behavioral experiments showed that synaptic interference carries an important biological meaning. For pairs of odors where we observed synaptic interference in physiological experiments, an association formed with one of those stimuli generalizes to the other odor. In other words, generalization arises because learning one association modifies representations of stimuli with overlapping response patterns. Thus, our results reveal important aspects of learning in a system with distributed population-level representations of sensory inputs, likely to be widely applicable to other memory-related brain areas.

Experimental Procedures

Flies

Our general strategy was to use highly specific split-GAL4 drivers to express CsChrimson (Klapoetke et al., 2014) in particular DANs while using less specific LexA drivers to label MBONs with GFP for electrode targeting. MB099C (TH-p65ADZp in VK00027, 73F07-ZpGAL4DBD in attP2) and MB320C (TH-p65ADZp in VK00027, 22B12-ZpGAL4DBD in attP2) were designed and constructed as previously described based on GAL4-line expression patterns (Aso et al., 2014a; Jenett et al., 2012; Pfeiffer et al., 2010). We needed to use MB320C as a driver for PPL1-γ1pedc rather than MB438B, which was previously described as a specific driver for that cell type (Aso et al., 2014a), because of concerns about transvection. MB438B has a p65ADZp insertion in attP40, the same site as the LexA lines we used (see below), and this can lead to expression of both LexA a GAL4 transcription factors in the same cells (Mellert and Truman, 2012). Flies bearing both split-GAL4 and LexA drivers were crossed with 13xLexAop-IVS-GFP-p10 (su(Hw)attP5); 20xUAS-CsChrimson-mVenus (attP2) for electrophysiology or 13xLexAop-IVS-GCaMP6f-p10

(su(Hw)attP5); 20xUAS-CsChrimson-mVenus (attP2) for imaging. For both electrophysiology and imaging, flies were raised at room temperature on conventional cornmeal-based medium. The resulting F1 females were collected on the day of eclosion, transferred to a food vial containing all-trans retinal (0.5 mM) and then kept in the dark for 36-72 hrs before being used for experiments. R12G04-LexA (attP40) was used for labeling MBON-γ1pedc, R25D01-LexA (attP40) for MBON-γ2α'1, R34B02-LexA (attP40) for MBON-α2sc, R14H06-LexA for γ KCs, and R13F02-LexA for pan-KCs. Expression patterns of split-GAL4 drivers used for DANs are shown in Figure S1. For behavior, crosses were kept on standard cornmeal food supplemented with retinal (0.2 mM all-trans-retinal prior to eclosion and then 0.4 mM) at 22°C at 60% relative humidity in a dark chamber.

Electrophysiology

In vivo whole-cell recordings were performed as previously reported (Wilson et al., 2004). The patch pipettes were pulled for a resistance of 5-7 Mω and filled with pipette solution containing (in mM): L-potassium aspartate, 125; HEPES, 10; EGTA, 1.1; $CaCl_2$, 0.1; Mg-ATP, 4; Na-GTP, 0.5; biocytin hydrazide, 13; with pH adjusted to 7.3 with KOH (265 mOsm). The preparation was continuously perfused with saline containing (in mM): NaCl, 103; KCl, 3; $CaCl_2$, 1.5; $MgCl_2$, 4; $NaHCO_3$, 26; N-tris(hydroxymethyl) methyl-2-aminoethane-sulfonic acid, 5; NaH_2PO_4, 1; trehalose, 10; glucose, 10 (pH 7.3 when bubbled with 95% O_2 and 5% CO_2, 275 mOsm). Whole-cell recordings were made using the Axon MultiClamp 700B amplifier (Molecular Devices). Specific cell types were visually targeted by GFP signal with a 60× water-immersion objective (LUMPlanFl/IR; Olympus) attached to an upright microscope (BX51WI; Olympus). Since the cell body of MBON-γ2α'1 was located ventral to the antennal lobes, we had to rotate the head by 180-degrees at the neck to expose the ventral side of the brain for recording, as described previously (Liu and Wilson, 2013). In current-clamp recordings, cells were held at around -60 mV by injecting hyperpolarizing current (< 50 pA). In some experiments, we also made cell-attached recordings using bath saline as pipette solution. Since the effects on spikes were indistinguishable between whole-cell and cell-attached recordings, we present them as one data set. The number of cell-attached recordings included in each figure is as follows: Figure 1 (E and F), *n* = 1; Figure 1(I and J), *n* = 1; Figure 7 (D and E), *n* =1; Figure 7 (G and H), *n* = 2; Figure S3, *n* = 1. For voltage-clamp recordings, we used a cesium-based pipette solution containing (in mM): cesium aspartate, 140; HEPES, 10; EGTA, 1; KCl, 1; Mg-ATP, 4; Na-GTP, 0.5; biocytin hydrazide, 13; QX-314, 10; with pH adjusted to 7.3 with CsOH (265 mOsm). To facilitate complete block of spikes, we used pipettes with a slightly larger tip opening (3-5 Mω); series resistance was maintained below 15 Mω and compensated for up to 80% through the amplifier's compensation circuitry. Cells were held at −70 or −60 mV, and cells that showed unclamped spikes during odor response were discarded. Signals were low-pass filtered at 5 kHz and digitized at 10 kHz.

Stimulus delivery

For odor delivery, a previously described custom-designed device was used (Honegger et al., 2011). Briefly, 40-ml vials were loaded with 5-ml pure odorants, and the saturated headspace vapors were diluted by two steps of air dilutions down to 1% (odor generalization experiments) or 2% (the rest of the experiments). Final flow rate of the air stream was set to

1 L/min with a final tubing size of 1/16 inch (inner diameter). Stability and reproducibility of the stimuli were continuously monitored throughout the experiments using a photo-ionization detector (PID; Aurora Scientific). The following chemicals were purchased from Sigma and used as stimuli: 3-octanol (CAS# 589-98-0), 4-methylcyclohexanol (589-91-3), pentyl acetate (628-63-7), butyl acetate (123-86-4), 2-heptanone (110-43-0) and ethyl lactate (97-64-3).

For photostimulation, a single red LED with peak wavelength of 627 nm (LXM2-PD01-0050; Philips) was custom-mounted on the microscope. Light pulses controlled by an LED driver (SLA-1200; Mightex) were presented to the brain at 14.7 mW/mm^2.

Pre-pairing odor responses were measured by presenting 1-s odor pulses with inter-stimulus interval of 25 s. In experimental situations with just two odors, they were presented alternately. When four odors were used, odors were presented in a pseudo-random order so that no odor was presented twice in succession. After recording a stable odor-response baseline, which typically took 5 trials (ranging from 3 to 10), odor-light pairing was performed 1 min after the last odor pulse of the pre-pairing series. Four light pulses (duration, 1 ms) were delivered at 2 Hz, starting 0.2 s after CS+ onset. In the 1-min pairing protocol, 120 light pulses were delivered at 2 Hz throughout the CS+ presentation. For experiments where only a single light pulse was used for pairing, the light was delivered 0.8 s after CS+ onset. The CS− was then presented 1 min after the CS+ pairing. Post-pairing odor responses were recorded starting 1 to 1.5 min after this CS− presentation. Each odor was presented typically 5 times, at least 3 times, in this post-pairing period, again in an interleaved manner with other odors.

Calcium Imaging

In vivo two-photon calcium imaging was performed as described previously (Campbell et al., 2013; Honegger et al., 2011). To stabilize the brain, the bath saline was replaced with a drop of saline containing 5% high-gelling point agarose (Cambrex Nusieve, catalog # 50080) held at 36°C. A circular coverslip (5mm diameter) was placed on the agarose drop to flatten the surface but removed later to prevent back-reflections of the stimulation light. We used a custom-built microscope with ScanImage (Vidrio Technologies) and a Ti-Sapphire laser (Chameleon XR; Coherent) tuned to 920 nm (8 to 14 mW at the sample). Images were collected with a 20×, NA 1.0 water-immersion objective lens (Olympus XLUMPLFLN) along with a Hamamatsu R3896 PMT. Imaging frames were typically 255x256 pixels, acquired with a pixel dwell time of 1.6 σs at average frame rates of 4.8 Hz. For photostimulation, we introduced light from an LED (the same one as for electrophysiology) into the excitation pathway, with the PMT protected from over-exposure by an emission filter (Semrock, Brightline FF01-520/70). Four pre- and post-pairing trials (imaging duration, 21 s) were alternately recorded for each odor (OCT and MCH), with a typical inter-stimulus interval of 40 s. Pairing was performed in the same manner as the electrophysiology experiments, using OCT as CS+. In some cases, a maximum of one trial from each of the trial groups had to be dropped from the analysis due to sample motion.

Data analysis

Electrophysiology—All the data analyses including statistical tests were performed in MATLAB (R2014a, MathWorks). Spikes were automatically detected by custom-written scripts by first removing slow membrane potential deflections with a high pass filter, and then identifying spikes based on amplitude, and verifying by visual inspection. PSTHs were calculated by convolving spikes with a Gaussian kernel (SD = 50 ms). Odor-evoked spikes were counted within the time window of 0 to 1.4 sec from odor onset. Spontaneous spiking rates were subtracted. EPSC charge transfer was calculated using the same time window. For the data from voltage-clamp recordings with potassium-based internal solution, current surges associated with unclamped action potentials were removed by low-pass filtering with cut-off frequency of 100 Hz before calculating the charge transfer. To determine the KC spike threshold, we used a ramp of current injection (slope 20 pA/s) to evoke a train of spikes. We detected the shoulder of the first spike in the train by searching for the first time point when the change in membrane potential exceeded 3 V/s, which empirically matched results of visual inspection for the membrane potential inflection point. To calculate the sustained spike rate, we counted the number of spikes evoked by a 1-s square pulse of current injection of 15-pA amplitude, which roughly corresponded to 1.5 times the average spike threshold current.

Calcium imaging—Analysis was performed as described previously (Campbell et al., 2013; Honegger et al., 2011). After motion-correction, each ROI (i.e. KC cell body) was manually selected (82 ± 9 cells per fly, mean ± SD; $n = 7$). To calculate F/F, baseline fluorescence was estimated by averaging frames prior to stimulus onset (5 s). Cells were judged to exhibit a significant response on a particular trial when the peak F/F in the response window (0.5 to 4.5 s after stimulus onset) calculated after filtering (five-frame moving average) was greater than 2.33 SDs of the baseline period. Significantly responsive cells for a given odor were defined as those that crossed this threshold in at least half of the trials. Response amplitude was calculated as the average F/F in the response window. We observed small decreases in the response magnitudes over the course of the experiments (Figure 2E). These were clearly unrelated to pairing because we observed similar reductions without photostimulation. The small decrease is likely attributable to technical factors related to imaging, such as photobleaching and photodamage of the GCaMP6f. Population representations were analyzed as a vector of the response amplitudes from all of the cells in a single imaging experiment. In other words, the odor representation on a given trial was the point defined by taking the response amplitude of each neuron on its corresponding axis in a multidimensional space where each dimension corresponds to a cell. For each odor, we computed Euclidean distances between post-pairing trials and the centroid of pre-pairing trials (pre-centroid) in this space as a measure of the change of population representations after pairing. Each distance was normalized to the distance of the pre-centroid from the origin. Note that analyzing the data without normalizing Euclidean distances also gave qualitatively similar results and we did not observe a statistically significant difference between CS+ and CS− (p = 0.58). We also computed cosine distances and the closely related Pearson's correlation between the post-pairing trials and the pre-centroid, and again we did not observe a significant difference between CS+ and CS− (p > 0.5 in each case). To

visualize these patterns in a 2D space, we used principal component analysis; the first two principal components captured 54% and 22% of the total variance, respectively.

See Supplemental Experimental Procedures for the description of behavior assay.

Supplementary Material

Refer to Web version on PubMed Central for supplementary material.

Acknowledgements

References

Akalal D-BG, Yu D, Davis RL. A late-phase, long-term memory trace forms in the γ neurons of Drosophila mushroom bodies after olfactory classical conditioning. J Neurosci. 2010; 30:16699–16708. [PubMed: 21148009]

Akalal D-BG, Yu D, Davis RL. The long-term memory trace formed in the Drosophila α/β mushroom body neurons is abolished in long-term memory mutants. J Neurosci. 2011; 31:5643–5647. [PubMed: 21490205]

Aso Y, Grübel K, Busch S, Friedrich AB, Siwanowicz I, Tanimoto H. The mushroom body of adult Drosophila characterized by GAL4 drivers. J. Neurogenet. 2009; 23:156–172. [PubMed: 19140035]

Aso Y, Hattori D, Yu Y, Johnston RM, Iyer NA, Ngo T-T, Dionne H, Abbott L, Axel R, Tanimoto H, et al. The neuronal architecture of the mushroom body provides a logic for associative learning. Elife. 2014a; 3:e04577. [PubMed: 25535793]

Aso Y, Herb A, Ogueta M, Siwanowicz I, Templier T, Friedrich AB, Ito K, Scholz H, Tanimoto H. Three dopamine pathways induce aversive odor memories with different stability. PLoS Genet. 2012; 8:e1002768. [PubMed: 22807684]

Aso Y, Sitaraman D, Ichinose T, Kaun KR, Vogt K, Belliart-Guérin G, Plaçais P-Y, Robie AA, Yamagata N, Schnaitmann C, et al. Mushroom body output neurons encode valence and guide memory-based action selection in Drosophila. Elife. 2014b; 4:e04580. [PubMed: 25535794]

Aso Y, Siwanowicz I, Bräcker L, Ito K, Kitamoto T, Tanimoto H. Specific dopaminergic neurons for the formation of labile aversive memory. Curr. Biol. 2010; 20:1445–1451. [PubMed: 20637624]

Blum AL, Li W, Cressy M, Dubnau J. Short- and long-term memory in Drosophila require cAMP signaling in distinct neuron types. Curr. Biol. 2009; 19:1341–1350. [PubMed: 19646879]

Boto T, Louis T, Jindachomthong K, Jalink K, Tomchik SM. Dopaminergic Modulation of cAMP Drives Nonlinear Plasticity across the Drosophila Mushroom Body Lobes. Curr. Biol. 2014; 24:822–831. [PubMed: 24684937]

Bouzaiane E, Trannoy S, Scheunemann L, Plaçais P-Y, Preat T. Two independent mushroom body output circuits retrieve the six discrete components of Drosophila aversive memory. Cell Rep. 2015; 11:1280–1292. [PubMed: 25981036]

Burke CJ, Huetteroth W, Owald D, Perisse E, Krashes MJ, Das G, Gohl D, Silies M, Certel S, Waddell S. Layered reward signalling through octopamine and dopamine in Drosophila. Nature. 2012; 492:433–437. [PubMed: 23103875]

Campbell RAA, Honegger KS, Qin H, Li W, Demir E, Turner GC. Imaging a population code for odor identity in the Drosophila mushroom body. J. Neurosci. 2013; 33:10568–10581. [PubMed: 23785169]

Cassenaer S, Laurent G. Hebbian STDP in mushroom bodies facilitates the synchronous flow of olfactory information in locusts. Nature. 2007; 448:709–713. [PubMed: 17581587]

Cassenaer S, Laurent G. Conditional modulation of spike-timing-dependent plasticity for olfactory learning. Nature. 2012; 482:47–52. [PubMed: 22278062]

Claridge-Chang A, Roorda RD, Vrontou E, Sjulson L, Li H, Hirsh J, Miesenböck G. Writing memories with light-addressable reinforcement circuitry. Cell. 2009; 139:405–415. [PubMed: 19837039]

Davis RL. Olfactory memory formation in Drosophila: from molecular to systems neuroscience. Annu. Rev. Neurosci. 2005; 28:275–302. [PubMed: 16022597]

Dubnau J, Grady L, Kitamoto T, Tully T. Disruption of neurotransmission in Drosophila mushroom body blocks retrieval but not acquisition of memory. Nature. 2001; 411:476–480. [PubMed: 11373680]

Hammer M. An identified neuron mediates the unconditioned stimulus in associative olfactory learning in honeybees. Nature. 1993; 366:59–63. [PubMed: 24308080]

Hawkins RD, Byrne JH. Associative Learning in Invertebrates. Cold Spring Harb Perspect Biol. 2015; 7:a021709. [PubMed: 25877219]

Heisenberg M. Mushroom body memoir: from maps to models. Nat. Rev. Neurosci. 2003; 4:266–275. [PubMed: 12671643]

Hige T, Aso Y, Rubin GM, Turner GC. Plasticity-driven individualization of olfactory coding in mushroom body output neurons. Nature. 2015; 526:258–262. [PubMed: 26416731]

Honegger KS, Campbell RAA, Turner GC. Cellular-resolution population imaging reveals robust sparse coding in the Drosophila mushroom body. J. Neurosci. 2011; 31:11772–11785. [PubMed: 21849538]

Huetteroth W, Perisse E, Lin S, Klappenbach M, Burke C, Waddell S. Sweet taste and nutrient value subdivide rewarding dopaminergic neurons in Drosophila. Curr. Biol. 2015; 25:751–758. [PubMed: 25728694]

Ito K, Suzuki K, Estes P, Ramaswami M, Yamamoto D, Strausfeld NJ. The organization of extrinsic neurons and their implications in the functional roles of the mushroom bodies in Drosophila melanogaster Meigen. Learn. Mem. 1998; 5:52–77. [PubMed: 10454372]

Janak PH, Tye KM. From circuits to behaviour in the amygdala. Nature. 2015; 517:284–292. [PubMed: 25592533]

Jenett A, Rubin GM, Ngo T-TB, Shepherd D, Murphy C, Dionne H, Pfeiffer BD, Cavallaro A, Hall D, Jeter J, et al. A GAL4-driver line resource for Drosophila neurobiology. Cell Rep. 2012; 2:991–1001. [PubMed: 23063364]

Keene AC, Waddell S. Drosophila olfactory memory: single genes to complex neural circuits. Nat. Rev. Neurosci. 2007; 8:341–354. [PubMed: 17453015]

Keene AC, Stratmann M, Keller A, Perrat PN, Vosshall LB, Waddell S. Diverse odor-conditioned memories require uniquely timed dorsal paired medial neuron output. Neuron. 2004; 44:521–533. [PubMed: 15504331]

Kim Y-C, Lee H-G, Han K-A. D1 dopamine receptor dDA1 is required in the mushroom body neurons for aversive and appetitive learning in Drosophila. J Neurosci. 2007; 27:7640–7647. [PubMed: 17634358]

Klapoetke NC, Murata Y, Kim SS, Pulver SR, Birdsey-Benson A, Cho YK, Morimoto TK, Chuong AS, Carpenter EJ, Tian Z, et al. Independent optical excitation of distinct neural populations. Nat Methods. 2014; 11:338–346. [PubMed: 24509633]

Krashes MJ, DasGupta S, Vreede A, White B, Armstrong JD, Waddell S. A neural circuit mechanism integrating motivational state with memory expression in Drosophila. Cell. 2009; 139:416–427. [PubMed: 19837040]

Krashes MJ, Keene AC, Leung B, Armstrong JD, Waddell S. Sequential use of mushroom body neuron subsets during drosophila odor memory processing. Neuron. 2007; 53:103–115. [PubMed: 17196534]

Lin AC, Bygrave AM, de Calignon A, Lee T, Miesenböck G. Sparse, decorrelated odor coding in the mushroom body enhances learned odor discrimination. Nat. Neurosci. 2014a; 17:559–568. [PubMed: 24561998]

Lin S, Owald D, Chandra V, Talbot C, Huetteroth W, Waddell S. Neural correlates of water reward in thirsty Drosophila. Nat. Neurosci. 2014b; 17:1536–1542. [PubMed: 25262493]

Liu C, Plaçais P-Y, Yamagata N, Pfeiffer BD, Aso Y, Friedrich AB, Siwanowicz I, Rubin GM, Preat T, Tanimoto H. A subset of dopamine neurons signals reward for odour memory in Drosophila. Nature. 2012; 488:512–516. [PubMed: 22810589]

Liu WW, Wilson RI. Glutamate is an inhibitory neurotransmitter in the Drosophila olfactory system. Proc. Natl. Acad. Sci. USA. 2013; 110:10294–10299. [PubMed: 23729809]

MacLeod K, Bäcker A, Laurent G. Who reads temporal information contained across synchronized and oscillatory spike trains? Nature. 1998; 395:693–698. [PubMed: 9790189]

Mao Z, Davis RL. Eight different types of dopaminergic neurons innervate the Drosophila mushroom body neuropil: anatomical and physiological heterogeneity. Frontiers in Neural Circuits. 2009; 3:5. [PubMed: 19597562]

Mauelshagen J. Neural correlates of olfactory learning paradigms in an identified neuron in the honeybee brain. J. Neurophysiol. 1993; 69:609–625. [PubMed: 8459289]

McGuire SE, Le PT, Davis RL. The role of Drosophila mushroom body signaling in olfactory memory. Science. 2001; 293:1330–1333. [PubMed: 11397912]

McGuire SE, Deshazer M, Davis RL. Thirty years of olfactory learning and memory research in Drosophila melanogaster. Prog Neurobiol. 2005; 76:328–347. [PubMed: 16266778]

Mellert DJ, Truman JW. Transvection is common throughout the Drosophila genome. Genetics. 2012; 191:1129–1141. [PubMed: 22649078]

Murthy M, Fiete I, Laurent G. Testing odor response stereotypy in the Drosophila mushroom body. Neuron. 2008; 59:1009–1023. [PubMed: 18817738]

Musso P-Y, Tchénio P, Preat T. Delayed dopamine signaling of energy level builds appetitive long-term memory in Drosophila. Cell Rep. 2015; 10:1023–1031. [PubMed: 25704807]

Okada R, Rybak J, Manz G, Menzel R. Learning-related plasticity in PE1 and other mushroom body-extrinsic neurons in the honeybee brain. J Neurosci. 2007; 27:11736–11747. [PubMed: 17959815]

Oleskevich S, Clements JD, Srinivasan MV. Long-term synaptic plasticity in the honeybee. J. Neurophysiol. 1997; 78:528–532. [PubMed: 9242301]

Olshausen BA, Field DJ. Sparse coding of sensory inputs. Curr. Opin. Neurobiol. 2004; 14:481–487. [PubMed: 15321069]

Owald D, Felsenberg J, Talbot CB, Das G, Perisse E, Huetteroth W, Waddell S. Activity of defined mushroom body output neurons underlies learned olfactory behavior in Drosophila. Neuron. 2015; 86:417–427. [PubMed: 25864636]

Pai T-P, Chen C-C, Lin H-H, Chin A-L, Lai JS-Y, Lee P-T, Tully T, Chiang A-S. Drosophila ORB protein in two mushroom body output neurons is necessary for long-term memory formation. Proc. Natl. Acad. Sci. USA. 2013; 110:7898–7903. [PubMed: 23610406]

Pech U, Pooryasin A, Birman S, Fiala A. Localization of the Contacts Between Kenyon Cells and Aminergic Neurons in the Drosophila melanogaster Brain Using SplitGFP Reconstitution. J. Comp. Neurol. 2013; 521:3992–4026. [PubMed: 23784863]

Perez-Orive J, Mazor O, Turner GC, Cassenaer S, Wilson RI, Laurent G. Oscillations and sparsening of odor representations in the mushroom body. Science. 2002; 297:359–365. [PubMed: 12130775]

Perisse E, Yin Y, Lin AC, Lin S, Huetteroth W, Waddell S. Different kenyon cell populations drive learned approach and avoidance in Drosophila. Neuron. 2013; 79:945–956. [PubMed: 24012007]

Pfeiffer BD, Ngo T-TB, Hibbard KL, Murphy C, Jenett A, Truman JW, Rubin GM. Refinement of tools for targeted gene expression in Drosophila. Genetics. 2010; 186:735–755. [PubMed: 20697123]

Plaçais P-Y, Trannoy S, Friedrich AB, Tanimoto H, Preat T. Two pairs of mushroom body efferent neurons are required for appetitive long-term memory retrieval in Drosophila. Cell Rep. 2013; 5:769–780. [PubMed: 24209748]

Qin H, Cressy M, Li W, Coravos JS, Izzi SA, Dubnau J. Gamma neurons mediate dopaminergic input during aversive olfactory memory formation in Drosophila. Curr. Biol. 2012; 22:608–614. [PubMed: 22425153]

Riemensperger T, Völler T, Stock P, Buchner E, Fiala A. Punishment prediction by dopaminergic neurons in Drosophila. Curr. Biol. 2005; 15:1953–1960. [PubMed: 16271874]

Schroll C, Riemensperger T, Bucher D, Ehmer J, Völler T, Erbguth K, Gerber B, Hendel T, Nagel G, Buchner E, et al. Light-induced activation of distinct modulatory neurons triggers appetitive or aversive learning in Drosophila larvae. Curr. Biol. 2006; 16:1741–1747. [PubMed: 16950113]

Schwaerzel M, Monastirioti M, Scholz H, Friggi-Grelin F, Birman S, Heisenberg M. Dopamine and octopamine differentiate between aversive and appetitive olfactory memories in Drosophila. J Neurosci. 2003; 23:10495–10502. [PubMed: 14627633]

Séjourné J, Plaçais P-Y, Aso Y, Siwanowicz I, Trannoy S, Thoma V, Tedjakumala SR, Rubin GM, Tchénio P, Ito K, et al. Mushroom body efferent neurons responsible for aversive olfactory memory retrieval in Drosophila. Nat. Neurosci. 2011; 14:903–910. [PubMed: 21685917]

Stettler DD, Axel R. Representations of odor in the piriform cortex. Neuron. 2009; 63:854–864. [PubMed: 19778513]

Tanaka NK, Tanimoto H, Ito K. Neuronal assemblies of the Drosophila mushroom body. J. Comp. Neurol. 2008; 508:711–755. [PubMed: 18395827]

Tomchik SM, Davis RL. Dynamics of learning-related cAMP signaling and stimulus integration in the Drosophila olfactory pathway. Neuron. 2009; 64:510–521. [PubMed: 19945393]

Turner GC, Bazhenov M, Laurent G. Olfactory representations by Drosophila mushroom body neurons. J. Neurophysiol. 2008; 99:734–746. [PubMed: 18094099]

Wang Y, Mamiya A, Chiang A-S, Zhong Y. Imaging of an early memory trace in the Drosophila mushroom body. J Neurosci. 2008; 28:4368–4376. [PubMed: 18434515]

Wilson RI, Turner GC, Laurent G. Transformation of olfactory representations in the Drosophila antennal lobe. Science. 2004; 303:366–370. [PubMed: 14684826]

Yamagata N, Ichinose T, Aso Y, Plaçais P-Y, Friedrich AB, Sima RJ, Preat T, Rubin GM, Tanimoto H. Distinct dopamine neurons mediate reward signals for short- and long-term memories. Proc. Natl. Acad. Sci. USA. 2014; 112:578–583. [PubMed: 25548178]

Yu D, Akalal D-BG, Davis RL. Drosophila alpha/beta mushroom body neurons form a branch-specific, long-term cellular memory trace after spaced olfactory conditioning. Neuron. 2006; 52:845–855. [PubMed: 17145505]

Zhang S, Roman G. Presynaptic inhibition of gamma lobe neurons is required for olfactory learning in Drosophila. Curr. Biol. 2013; 23:2519–2527. [PubMed: 24291093]
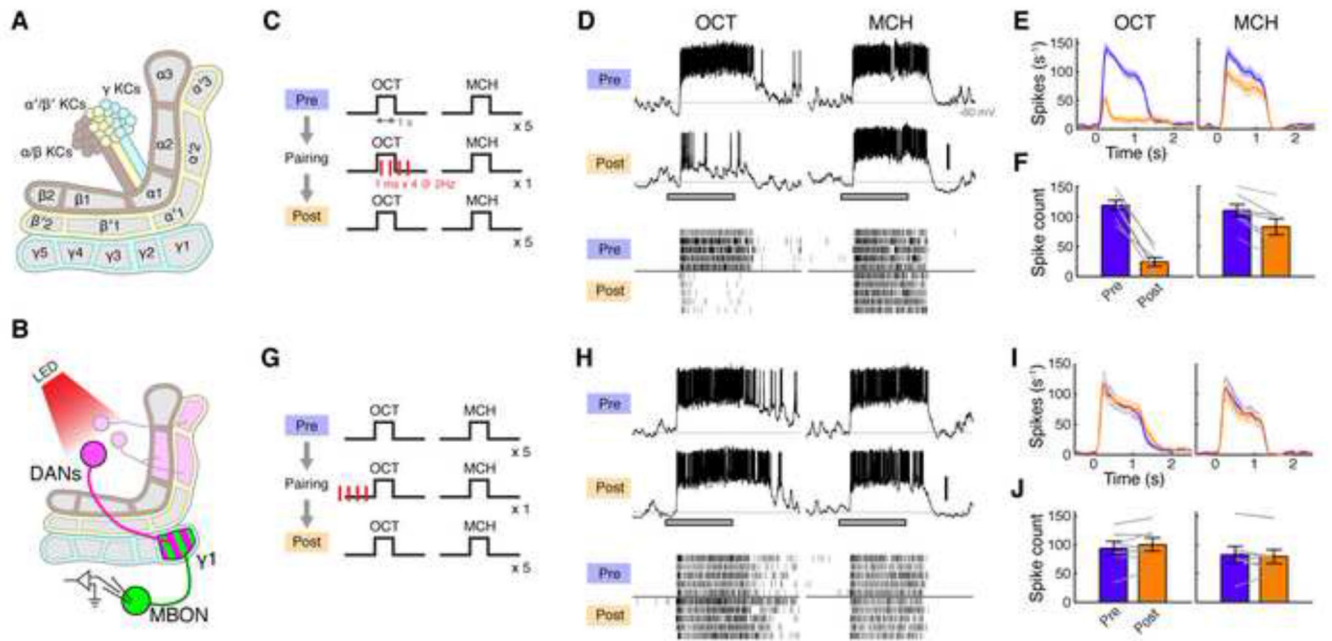
Figure 1. Forward Pairing of Odor and DAN Activation Induces Long-lasting Suppression in the γ1 Compartment

(A) Schematic of MB lobes showing DAN-MBON compartments.

(B) Expression of CsChrimson and GFP was driven by MB320C and R12G04-LexA, respectively. Recordings were made from MBON-γ1pedc.

(C) Forward pairing protocol. Four light pulses (1 ms in duration) were delivered at 2 Hz, starting 0.2 s after CS+ onset.

(D) Representative single-cell data, showing odor responses before (Pre) and after (Post) pairing. Gray bar, 1-s odor presentation. Scale bar, 20 mV. Raster plots (bottom) show spikes.

(E) Mean spike rates over several experiments displayed as peristimulus time histogram (PSTH; ± SEM, shaded area; $n = 7$).

(F) Mean odor-evoked spike count (± SEM). Gray lines indicate data from individual flies. Spike counts decreased in both CS+ (OCT, $p < 10^{-4}$, Tukey's *post hoc* test) and CS− (MCH, $p < 0.01$), but the effect of pairing was significantly different between odors ($p < 0.001$, repeated measures two-way ANOVA).

(G) Backward pairing protocol. Odor was delivered 0.5 s after the last pulse of light.

(H) Representative single-cell data.

(I) Mean PSTH ($n = 7$).

(J) Mean odor-evoked spike count. Backward pairing showed no effect ($p > 0.05$, repeated measures two-way ANOVA).
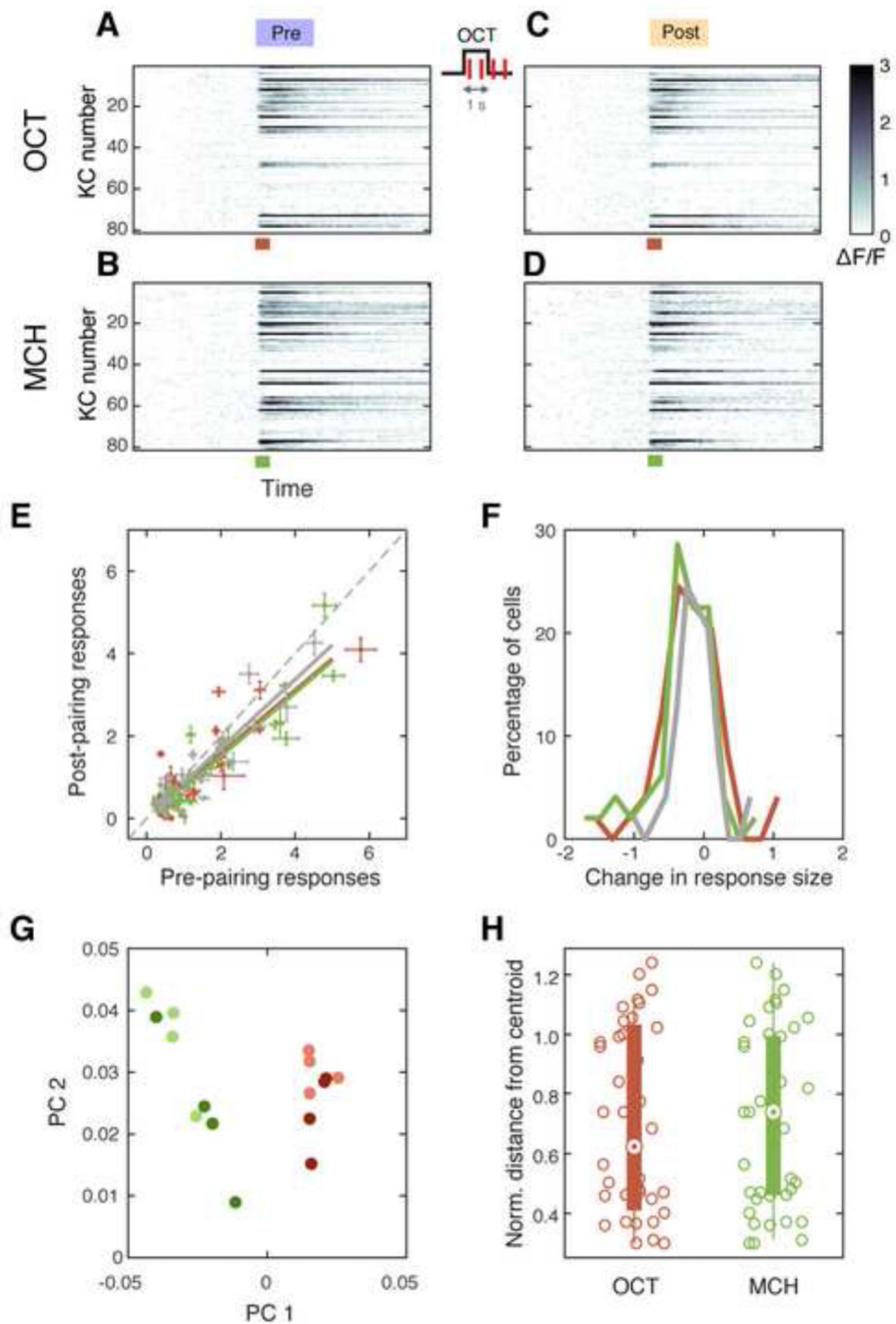
Figure 2. Odor-Dopamine Pairing does Not Change KC Odor Responses

(A-D) Trial-averaged time courses (4 trials) of odor responses (F/F, pseudo color) in KCs before (A, C) and after (B, D) 1-s odor-light pairing. Data from a single representative fly. Each row corresponds to a single KC. Colored bars, 1-s odor presentation.

(E) Median response amplitude for each significantly responding cell before and after pairing. Red and green points indicate CS+ (OCT; *n* = 53 cells from 5 flies) and CS− (MCH; *n* = 49) respectively. Gray points are from control experiments where no light pulses were delivered (OCT and MCH; *n* = 32 from 2 flies). Error bar, median absolute deviation. Solid

lines, linear regressions. Dashed line, unity. All three data set showed small but significant decrease after pairing ($p < 0.05$, paired t-test).

(F) Histograms of the change in response magnitude (F/F) after pairing (pre subtracted from post). Only cells that significantly responded to the odor in either pre- or post-pairing recordings were included. There was no difference between any combination of the distributions of CS+ responses (red), CS− (green) and control (gray; Kolmogorov Smirnov test, $p > 0.1$).

(G) Single-trial responses projected onto the space of the first two principal components. Data from a single representative fly. Responses from pre- (lighter colors) and post-pairing trials (darker colors) are intermingled, while CS+ (red) and CS− (green) are well-separated.

(H) Comparing population response patterns pre- and post-training. Euclidean distances between each post-pairing trial and the centroid of pre-pairing trials calculated in the full n-dimensional neuronal representation space are plotted, where n corresponds to the number of neurons imaged in each fly. Distances were normalized to the distance from the origin to the centroid of the pre-pairing trials. There was no significant difference between CS+ (red) and CS− (green; $p = 0.58$, unpaired t-test). See also Experimental Procedures.
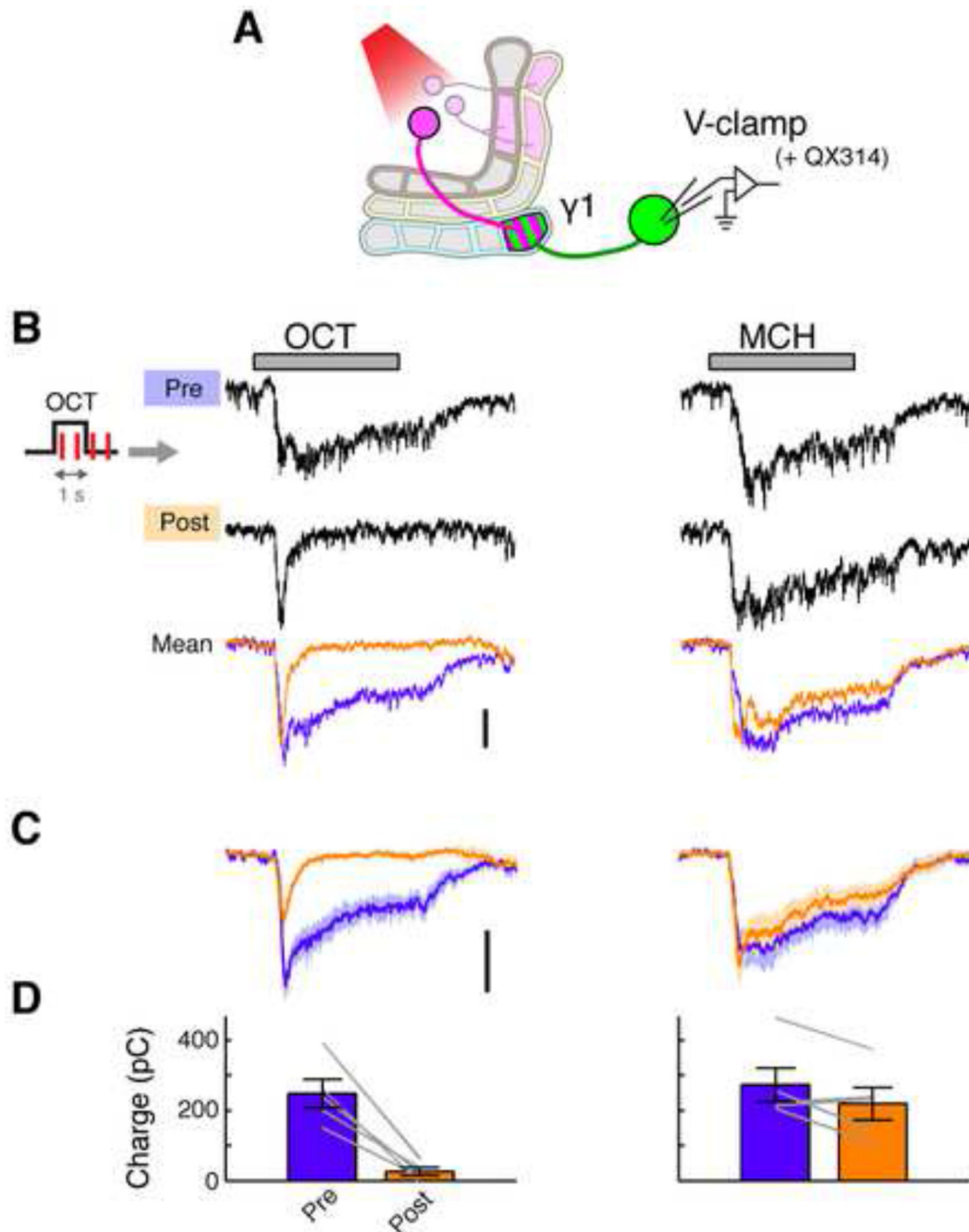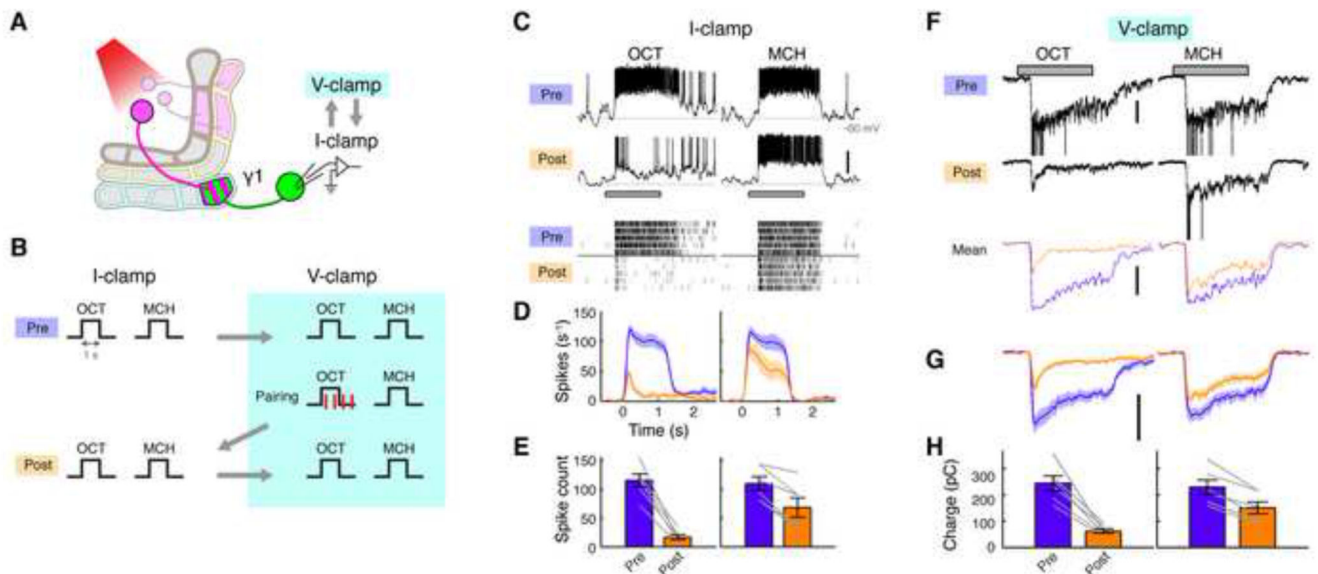
Figure 3. Pairing of Odor and DAN Activation Induces Synaptic LTD
(A) Expression of CsChrimson and GFP was driven by MB320C and R12G04-LexA, respectively. Whole-cell voltage-clamp recordings were made from MBON-γ1pedc. Action potentials were completely suppressed by QX-314 in the pipette solution.
(B) Representative voltage-clamp data from a single cell, showing odor-evoked EPSCs before (Pre) and after (Post) pairing. Gray bar, 1-s odor presentation. Overlaid traces (bottom) show mean EPSCs pre- and post-pairing in this cell (n = 5-7 trials). Scale bar, 200 pA.

(C) Mean EPSCs (± SEM, shaded area; $n = 5$ cells).

(D) Mean charge transfer of EPSC (± SEM). Gray lines indicate data from individual flies. Excitatory synaptic input decreased for CS+ ($p < 0.005$, Tukey's *post hoc* test following repeated measures two-way ANOVA) but not for CS− ($p > 0.1$).

Figure 4. Postsynaptic Spikes are Dispensable for LTD Induction

(A) Expression of CsChrimson and GFP was driven by MB320C and R12G04-LexA, respectively. Whole-cell recordings were made from MBON-γ1pedc.

(B) After recording baseline odor responses in current-clamp mode, recording mode was switched to voltage clamp to record EPSCs. Odor-light pairing (1-s odor with 1-ms light pulses × 4) was performed under voltage-clamp mode, which suppressed 83 ± 4.5 % of odor-evoked spikes (mean $\pm$ SEM, $n = 6$). After pairing, spikes and EPSCs were recorded by flipping the mode between current-clamp and voltage-clamp.

(C) Representative current-clamp data from a single cell, showing odor responses before (Pre) and after (Post) pairing. Gray bar, 1-s odor presentation. Scale bar, 20 mV. Raster plots (bottom) show spikes.
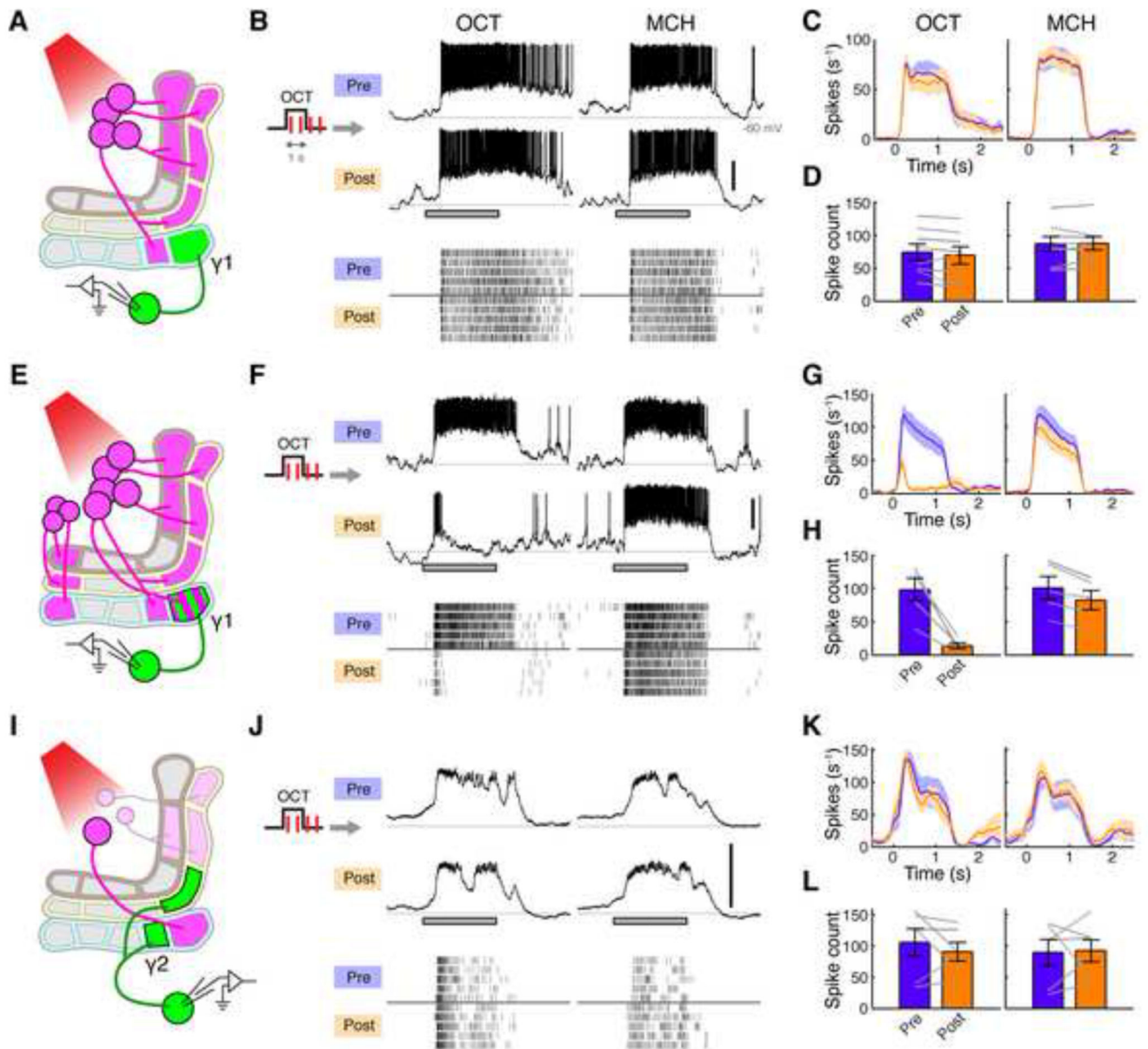
(D) Mean PSTH ($\pm$ SEM, shaded area; $n = 6$).

(E) Mean odor-evoked spike count ($\pm$ SEM). Gray lines indicate data from individual flies. Spike counts decreased in both CS+ ($p < 0.001$, Tukey's *post hoc* test) and CS− ($p < 0.01$), but the effect of pairing was significantly different between the two odors ($p < 0.005$, repeated measures two-way ANOVA).

(F) Representative voltage-clamp data from the same cell shown in (C). Currents evoked by unclamped spikes were truncated for display. Mean EPSCs (3 trials) after filtering out unclamped spikes are also shown (bottom). Scale bar, 200 pA.

(G) Mean filtered EPSCs ($\pm$ SEM, shaded area; $n = 6$).

(H) Mean charge transfer ($\pm$ SEM). Gray lines indicate data from individual flies. Charge transfer decreased in CS+ ($p < 0.001$, Tukey's *post hoc* test) and CS− ($p < 0.001$), but the effect of pairing was significantly different between the two odors ($p < 0.005$, repeated measures two-way ANOVA).

Figure 5. DAN-induced Plasticity is Compartment Specific

(A) Expression of CsChrimson and GFP was driven by MB099C and R12G04-LexA, respectively. Recordings were made from MBON-γ1pedc.

(B) Representative single-cell data, showing odor responses before (Pre) and after (Post) pairing. Gray bar, 1-s odor presentation. Scale bar, 20 mV. Raster plots (bottom) show spikes.

(C) Mean PSTH (± SEM, shaded area; $n = 8$).

(D) Mean odor-evoked spike count (± SEM). Gray lines indicate data from individual flies. Pairing had no significant effect ($p > 0.05$, repeated measures two-way ANOVA).

(E) Expression of CsChrimson was driven by TH-GAL4, which labels a broad subset of PPL1 DANs, including PPL1-γ1pedc, and a few PAM DANs as well as many other DANs outside the MB (not shown). Recordings were made from MBON-γ1pedc.

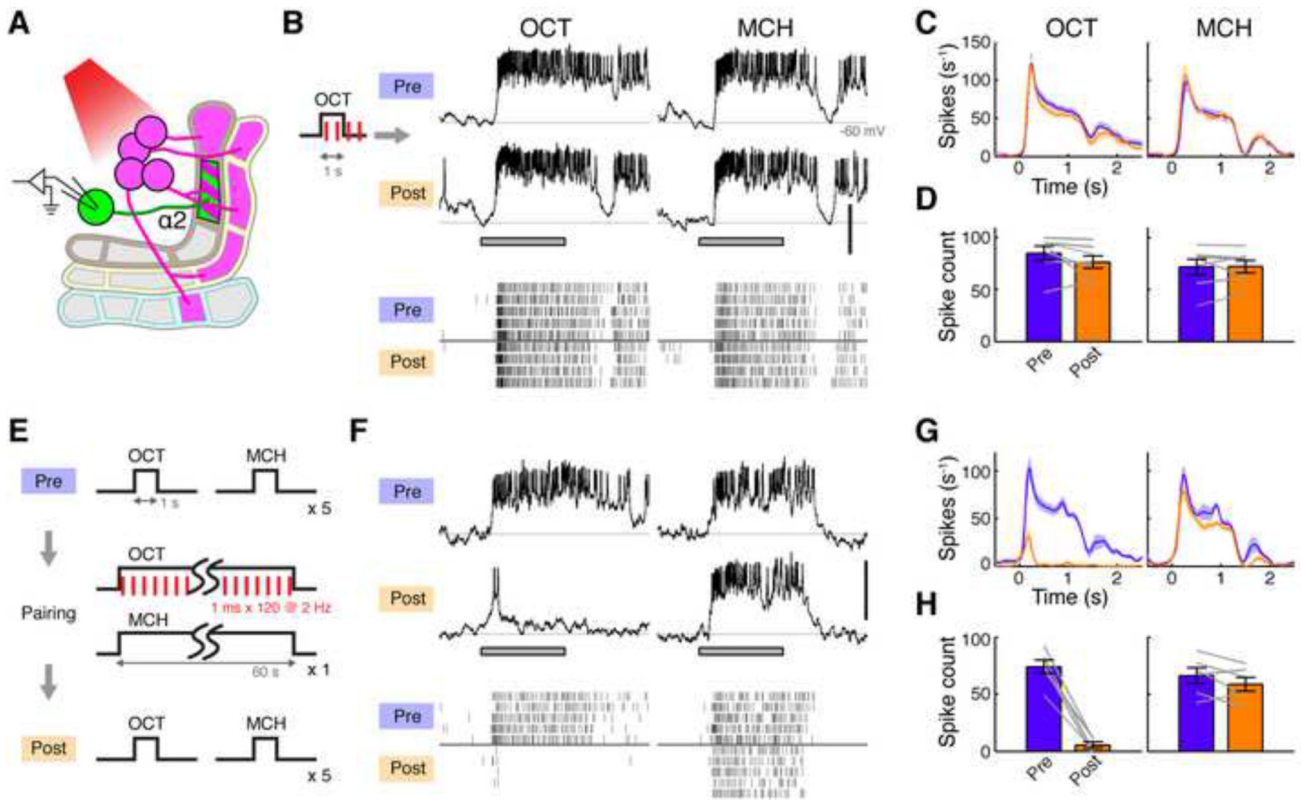(F) Representative single-cell data.

(G) Mean PSTH ($n = 5$).

(H) Mean odor-evoked spike count. Spike counts decreased in both CS+ ($p < 0.01$, Tukey's *post hoc* test) and CS− ($p < 0.01$), but the effect of pairing was significantly different between the two odors ($p < 0.05$, repeated measures two-way ANOVA).

(I) Expression of CsChrimson and GFP was driven by MB320C and R25D01-LexA, respectively. Recordings were made from MBON-γ2α'1.

(J) Representative single-cell data.

(K) Mean PSTH ($n = 6$).

(L) Mean odor-evoked spike count. Pairing showed no effect ($p > 0.1$, repeated measures two-way ANOVA).

Figure 6. Plasticity Rule is Different across Compartments

(A) Expression of CsChrimson and GFP was driven by MB099C and R34B02-LexA, respectively. Recordings were made from MBON-α2sc.

(B) Representative single-cell data, showing odor responses before (Pre) and after (Post) 1-sec pairing. Gray bar, 1-s odor presentation. Scale bar, 20 mV. Raster plots (bottom) show spikes.
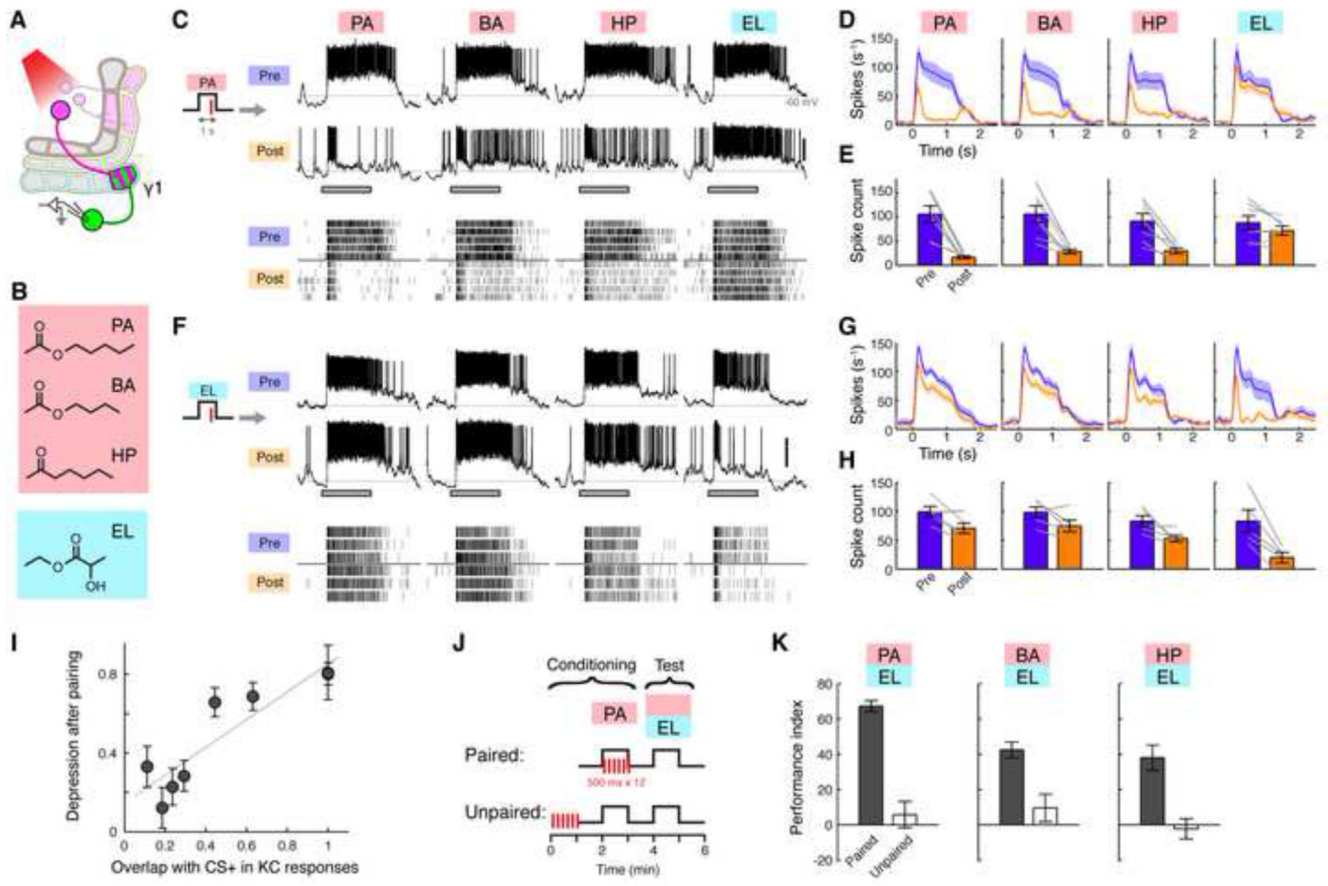
(C) Mean PSTH (± SEM, shaded area; $n = 7$).

(D) Mean odor-evoked spike count (± SEM). Gray lines indicate data from individual flies. Pairing showed no effect ($p > 0.1$, Tukey's *post hoc* test following repeated measures two-way ANOVA).

(E) 1-min pairing protocol.

(F) Representative single-cell data.

(G) Mean PSTH ($n = 6$).

(H) Mean odor-evoked spike count. Spike counts decreased in CS+ ($p < 10^{-5}$, Tukey's *post hoc* test) but not in CS− ($p > 0.1$), and the effect of pairing was significantly different between the two odors ($p < 0.001$, repeated measures two-way ANOVA).

Figure 7. Synaptic Interference and Olfactory Generalization

(A) Expression of CsChrimson and GFP was driven by MB320C and R12G04-LexA, respectively. Recordings were made from MBON-γ1pedc.

(B) Chemical structures of the test odors. PA: pentyl acetate, BA: butyl acetate, HP: 2-heptanone, EL: ethyl lactate.

(C) Representative single-cell data, showing odor responses before (Pre) and after (Post) pairing with PA. Gray bar, 1-s odor presentation. Gray line, −60 mV. Scale bar, 20 mV. Raster plots (bottom) show spikes.

(D) Mean PSTH (± SEM, shaded area; $n = 7$).

(E) Mean odor-evoked spike count (± SEM). Gray lines indicate data from individual flies. Depression was significant for PA, BA and HP ($p < 0.005$, Tukey's *post hoc* test following repeated measures two-way ANOVA) but not for EL ($p > 0.1$). Depression of PA was slightly stronger than BA and HP ($p < 0.05$, paired *t*-test).

(F) Representative single-cell data for pairing with EL.

(G) Mean PSTH ($n = 5$).

(H) Mean odor-evoked spike count. Depression was significant for EL ($p < 0.01$, Tukey's *post hoc* test following repeated measures two-way ANOVA) and HP ($p < 0.05$) but not for the others ($p > 0.05$). Depression of EL was stronger than HP ($p < 0.05$, paired *t*-test).

(I) Magnitude of depression correlates with extent of overlap in KC response patterns ($p < 0.005$, Pearson's $r = 0.90$). Each point shows the response depression for a different odor

with the indicated degree of overlap with the CS+ KC response pattern (overlap calculated from data in Campbell et al., 2013). Error bars, SEM. Gray line, linear regression.

(J) Behavioral test for odor generalization. Flies were presented with PA and light in a paired or unpaired manner (see Figure S1) and subsequently tested for aversive learning with one of the three different combinations of odors.

(K) Performance index (PI). Positive PI indicates relative avoidance of PA, BA or HP when flies are given the choice between those odors and EL. Flies generalized their avoidance of PA to the other odors ($n = 10$ for each; $p < 0.01$, Tukey's *post hoc* test following two-way ANOVA).